Journal of Materials Chemistry C

Accepted Manuscript

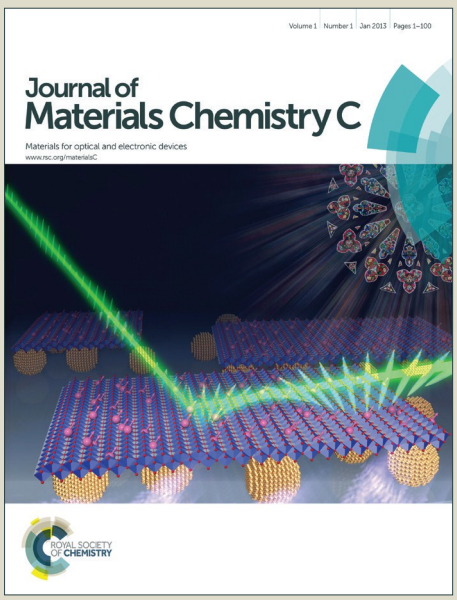

ROYAL SOCIETY OF CHEMISTRY

www.rsc.org/materialsC

Journal Name

ARTICLE TYPE

Cite this: DOI: 10.1039/xxxxxxxxxx

Nanoparticles dispersed in liquid crystals: Impact on conductivity, low-frequency relaxation and electro-optical performance†

Martin Urbanski* and Jan P. F. Lagerwall

Received Date
Accepted Date

DOI: 10.1039/xxxxxxxxxx

www.rsc.org/journalname

We study the impact of functionalized gold nanoparticles on the impedance response of nematic nanoparticle / liquid crystal dispersions in the frequency range of 0.1 Hz - 100 kHz. By fitting a suitable equivalent electric circuit model to the experimental data we show that nanoparticle doping does not affect the permittivity of the nematic host, but significantly increases its conductivity. This causes a Debye-type relaxation process in the Hz and low kHz regime, which originates from mobile charge carriers accumulating near the electrodes of the test cell. The effect of this electrode polarization on the electro-optical response of the nanocomposites is discussed with respect to threshold voltage and dielectric permittivity. We demonstrate that nanoparticle doping does not alter the electro-optic response at frequencies above the occurrence of electrode polarization, while it strongly deteriorates the performance in the low frequency regime.

1 Introduction

Functional composites of nanoparticles (NPs) dispersed in liquid crystals (LCs) have emerged into a topical research field as they offer great opportunities both for fundamental science and promising applications. In particular the impact of NPs on the electro-optical performance of nematic host materials is of considerable interest due to the importance and large scale production of LC displays. Despite the high activity in this field for over a decade, the complex interactions between dopant and host are not fully understood yet. A general approach for the design of high performing LC nanocomposites is still missing.

Promising advances in the understanding of NP-LC interactions were reported for composites with anisometric dopant-host interactions. Ferroelectric NPs were shown to increase the dielectric anisotropy[1] or the orientational order[2] due to the coupling of their dipole moment to the uniaxial order of the nematic host. Prasad et al. reported an enhancement of elastic, dielectric and conductivity anisotropy for dispersions containing gold nanorods[3] and attributed this behavior to the anisometric shape of the dopant. Carbon nanotubes, due to their high aspect ratios, were shown to align parallel to the director of nematic LCs[4] and induce a high anisotropy of conductivity to the host[5,6].

The behavior of spherical NPs was subject of our earlier studies, where we investigated the role of organic functionalization of NPs on the dispersibility in the nematic phase. Based on optical and electro-optical observations, we proposed a model of anisometrically distorted ligand shells adapting to the uniaxially ordered nematic phase[7,8]. This model links to established explanation models for anisometric particles and provides reasonable explanation to several doping effects of spherical particles, such as dispersibility limits[9] or changes of threshold voltage[10]. It is, however, still incomplete as it cannot reproduce a commonly reported relaxation phenomenon, typically observed in the low kHz regime. For example, Kobayashi and coworkers showed that this relaxation can be related to an unusal frequency dependence of threshold voltage for the switching of a twisted nematic liquid crystal display doped with metallic nanoparticles[11]. The authors attribute this observation to the formation of Maxwell-Wagner-Sillars polarization at the interface between each NP and the dielectric surrounding, and thus treat the nanoparticle dispersion as a heterogeneous dielectric medium. Similar experimental observations of a low frequency relaxation are reported by Yoshida et al.[12] for 5CB doped with gold nanoparticles via sputter doping. They discuss the polarization of the nanoparticles themselves as source for the Debye-type relaxation. Studying semiconducting CdS NPs in 5CB, Zhang et al. reported similar observations, in this case assuming that the origin is the impact of the spherical nanoparticles on the order parameter of the nematic host material rather than polarization effects[13].

Motivated by the discussion of electric polarization in NP-LC

University of Luxembourg, Physics & Materials Science Research Unit, 162a Avenue de la Faiencerie, Luxembourg, Luxembourg. Fax: +352 466644 36219; Tel: +352 466644 6732; E-mail: Martin.Urbanski@lc-science.info

† Electronic Supplementary Information (ESI) available: Polarizing optical microscopy study on the impact of nanoparticle doping on the alignment of NP-LC composites; detailed discussion of the derivation of an appropriate equivalent electrical circuit; effective medium considerations on the effect of metal NPs on the composite permittivity; Movie visualizing electrode polarization. See DOI: 10.1039/b000000x/

nanocomposites by Kobayashi[11] and Yoshida[12], we shift focus of our present study to rather indirect doping effects, such as contamination with impurities and their effect on conductivity and permittivity. Recent studies revealed already that nanoparticle doping can increase the conductivity of the nematic host by orders of magnitude, as reported by Tomylko et al. for diamond nanoparticles[14], Ha et al. for titanium nanoparticles[15] or Garcia-Garcia and coworkers for carbon nanotubes[16]. Our present study combines the analysis of polarization processes and conductivity for spherical gold nanoparticles and therefore contributes to a better understanding of particle-host interactions. We find that, as an alternative to the above mentioned explanations of the NP influence on the low frequency LC performance, a model for mobile charge carriers in confined space also yields an excellent reproduction of the experimental observations.

2 Materials and Methods

We utilize spherical gold nanoparticles with different organic functionalization: **NP1** features a dodecanethiol ligand shell and represents aliphatic functionalized NPs as used in the seminal studies by Qi and Hegmann[17,18], while **NP2** is capped with mesogenic ligands, which are expected to increase dispersibility and have stronger impact on the nematic host[19,20]. Both types of nanoparticles are expected to be non-conductive, since they do not carry any net charge and are electrically isolated by a dense, non-conducting organic ligand shell. Dodecanethiol functionalized gold nanoparticles **NP1** were purchased from Sigma-Aldrich as dispersion (2 % (w/v)) in toluene with average core sizes between 3-5 nm. Dispersions of **NP1** were prepared in 4-cyano-4'-pentylbiphenyl (5CB) by adding suitable amounts of the nanoparticle dispersion in toluene to a small amount of liquid crystal. The solvent was then removed at a temperature of 60°C and reduced pressure for 36 h. Liquid-crystal-decorated gold nanoparticles capped with 11-(4'cyanobiphenyl-4-yloxy)undecylthiol (**NP2**) were synthesized by Dr. Michael Draper following the Hutchison ligand exchange method[21] and were kindly provided for this study. The full characterization of these particles with average diameter of 2.40 nm can be found elsewhere[19]. Dispersions of **NP2** in 5CB were prepared by dissolving a small amount of **NP2** (3-5 mg) in dichloromethane (1500 μL) under mechanical stirring and slightly elevated temperatures (40°C). A suitable amount of the **NP2** dispersion was then added to a small amount of 5CB and the solvent was evaporated at 40°C and reduced pressure for 24 h. The nematic host 5CB was purchased from Synthon Chemicals GmbH and used without further purification. We choose impedance spectroscopy as a versatile tool to analyze electric polarization, permittivity and conductivity properties in composites of **NP1** and **NP2** in the nematic host 5CB. Dielectric spectroscopy measurements were performed using a high resolution Alpha Analyzer (Novocontrol GmbH) combined with Quatro temperature controller in the frequency range from 0.1 Hz - 100 kHz and a test level amplitude of 0.3 V. Threshold voltages and permittivities were measured on an E4980A impedance analyzer (Agilent) in combination with a Linkam TMS600 heating stage and CS90 controller at varying test level amplitudes from 5 mV to 19.85 V. For dielectric characterization, freshly prepared dispersions were filled at T=60°C into polyimide coated test cells (E.H.C. Co., Ltd, Japan) with 50 μm cell gap, 100 mm^2 electrode area and antiparallel rubbing for planar alignment.

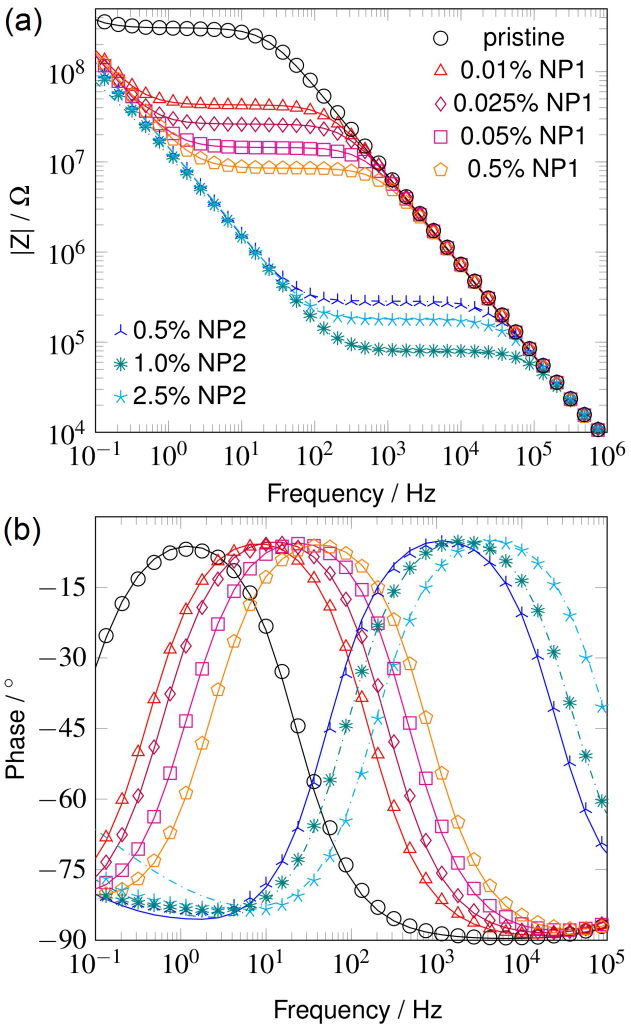

Fig. 1 Impedance (a) and phase angle (b) results for the pristine host 5CB and NP-LC dispersions doped with NP1 or NP2. Markers represent experimentally observed values, while lines were obtained via fitting the equivalent electrical circuit model shown in Fig. 2 to the experimental data.

3 Impedance spectroscopy

3.1 Experimental results

Experimental data for the impedance $|Z| = \sqrt{R^2 + X^2}$, with R the active component and X the reactive component of the complex resistance Z, and for the phase angle $\varphi = \mathrm{atan}(X/R)$ are summarized in Figure 1. All measurements were performed perpendicular to the director, see ESI† for additional information. The impedance of pristine 5CB exhibits a linear decrease in the log-log diagram for increasing frequencies over a broad range from 20 Hz - 1 MHz (black data set in Fig. 1a). Below 5 Hz the slope significantly flattens out and reaches a plateau of quasi-constant impedance at Z=306 MΩ. For frequencies < 0.2 Hz a slight in-

crease of impedance is observed. The phase angle (Fig. 1b) remains close to -90° for frequencies higher than 103 Hz. Below this frequency the phase angle steadily increases until it reaches its maximum at -7° at 1.15 Hz, which coincides with the saddle point of the impedance.

This impedance response is characteristic for a capacitor with small residual conductivity. Liquid crystals are typically considered good insulators, as highly purified nonionizing liquid crystals typically feature conductivities smaller than 10^{-13} - 10^{-10} Scm^{-1}.[22] Long time exposure to ambient conditions leads to the absorption of water and other impurities and may increase the conductivity by several orders of magnitude[14]. Additionally, the host 5CB, like most alkyl cyanobiphenyls, suffers from molecular degradation and intrinsically forms small amounts of ions. The conductivities of pristine 5CB at 25°C were determined to be $\sigma_{\perp}$=1.1x$10^{-10}$$Scm^{-1}$ and $\sigma_{\parallel}$=3.8x$10^{-10}$$Scm^{-1}$.

Impedance data for dispersions of dodecanethiol functionalized gold nanoparticles **NP1** in 5CB at different concentrations (0.01 %-0.5% (w/w)) are shown by the reddish ensemble of plots with open symbols in Figure 1. For frequencies above 3 kHz, the impedance coincides with that of pristine 5CB for all **NP1** doping concentrations. This indicates a dominating reactive component with similar capacitance as the pristine host. Below 3 kHz, the impedance of each **NP1** doped sample flattens to a quasi-constant plateau, which shifts to higher frequencies and lower impedances with increasing doping concentration. Such behavior is characteristic for a capacitor with increasing leakage current, here apparently correlated to higher doping concentrations. At low frequencies, $f < 0.6$ Hz, the impedance data of all **NP1** doped samples coincide again to a linear increase on the log-log scale, with identical slope to that in the high frequency regime. The change between capacitive and ohmic behavior is also reflected by the phase angle response: The phase angle tends towards -90° for high frequencies, where the impedance shows a linear decrease, and features a maximum at the frequency of the saddle point in $|Z|$. The evolution of phase angle over frequency for **NP1** doped samples is therefore similar to the pristine host, its shape maintained yet shifted to higher frequency values.

Dispersions containing the mesogen functionalized gold nanoparticles **NP2** (0.5%-2.5% (w/w)) show similar characteristics in their impedance spectra, as shown by the bluish ensemble of star symbol plots in Figure 1. As for the **NP1** doped samples, the phase angle of **NP2** dispersions maintains the characteristic shape, but is shifted towards higher frequencies. It shows a maximum at the frequency of a saddle point in the impedance response and tends towards -90° for frequency regimes where $|Z|$ shows a linear slope identical to that of the pristine host or of **NP1**-doped dispersions. Notably, the plateau of quasi-constant impedance is strongly shifted towards higher frequencies and occurs at significantly lower impedance values for comparable nanoparticle concentrations.

3.2 Equivalent electrical circuit analysis

For a more quantitative analysis we utilize an equivalent electrical circuit (EEC) model which reproduces the experimental impedance and phase angle data to analyze the dielectric spectra. Several EECs for modeling liquid crystal test cells have been reported in literature, varying in complexity and suitable frequency range. Simple approaches comprise a resistor R_{CR} for the resistivity of cell electrodes and connectors, in series with a parallel set of capacitor C_{LC} and resistor R_{LC}, resembling the active and reactive behavior of the liquid crystal[16]. Such simplified model achieves a sufficient accuracy only for mid-range frequency values between 100 Hz and 100 kHz and low residual conductivity. For modeling also the low frequency behavior in the range from 0.1 Hz − 100 Hz or samples with moderate conductivity, Sprokel introduced an EEC with a capacitance C_{DL} in series with the parallel combination of bulk capacitance C_{LC} and resistivity R_{LC}[23]. By adding the capacitance element C_{DL} in series to C_{LC} and R_{LC}, the possible accumulation of space-charge near the electrodes due to the confinment in a liquid crystal test cell is taken into account.

Belyaev and Drokin extended this EEC by a finite diffusion Warburg element W to model the drift of charged species through the dielectric LC slab and a resistor R_A and capacitance C_A in series for an adsorbed double layer of charged alignment agent, all three additional elements parallel to the surface capacitance[24]. More sophisticated models also succeed in modeling Debye dielectric relaxation at high frequencies in the MHz regime, but it has been reported that up to eight components are required where the physical meaning of every component is occasionally questionable[6]. By restricting the frequency range for our experiments to 0.1 Hz - 100 kHz, we avoid molecular relaxation and can use a simplified EEC where each component represents a meaningful physical process of the LC test cell. The EEC model used in this study resembles a combination of the three EEC models previously introduced and is shown in Figure 2 (see ESI† for further discussion).

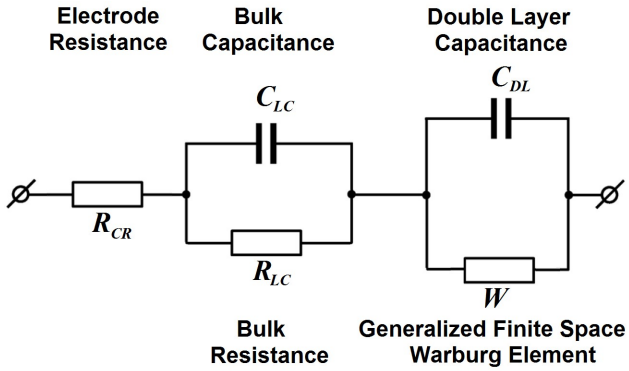

Fig. 2 Proposed equivalent electrical circuit model for a NP-LC filled test cell.

The capacitor C_{LC} in Figure 2 represents the reactive component of the liquid crystal bulk phase and is linked to the permittivity ε of the liquid crystal, while the resistor R_{LC} represents the active component of the bulk phase caused by residual impurities. R_{LC} can therefore be seen as a measure of the conductivity of the sample. In order to model the impedance response also in the low frequency regime, ion drift and accumulation of space-charge near the electrodes have to be taken into account. The

capacitance of the space charge is represented by the capacitor C_{DL}, while the drift of ions within confined geometry is modeled by a generalized finite space Warburg element W. Its impedance is given by $Z_W = \frac{W_{sr}}{\sqrt{\omega}}(1-j)tanh(W_{sc}\sqrt{j\omega})$ with the two parameters $W_{sr} = \frac{RTN_A}{F^2 S n_s \sqrt{2D}}$ and $W_{sc} = \frac{\delta_N}{\sqrt{D}}$, where R is the gas constant, T absolute temperature, N_A Avogadro's constant, F the Faraday constant, S the electrode area of the test cell, n_s the concentration of mobile ions on the surface, D the effective diffusion coefficient of mobile ions and δ_N the thickness of the Nernst diffusion layer[24,25]. The resistor R_{CR} represents the resistivity of connectors and electrodes and is needed to model the cell relaxation phenomenon in the high frequency regime, since the combination of R_{CR} and C_{LC} constitutes a low pass filter which leads to an RC cutoff at high frequencies with dominating active response (see ESI† for further discussion).

By fitting the EEC model to the experimental data we were able to reproduce the impedance spectra with high accuracy, as can be seen in Figure 1: While the open symbols indicate experimentally obtained data, the superimposed lines were obtained via EEC fitting. The resulting values for the components of the EEC model are summarized in Table 1. The resistance R_{CR}, representing the resistivity of connectors and electrodes, is unaffected by the presence of nanoparticles ($R_{CR} = 4.0 \pm 0.5 k\Omega$). Also the reactive component of the bulk C_{LC} remains constant upon the addition of dopant ($C_{LC} = 22.6 \pm 0.6 pF$), a small deviation expected from the slightly different cell gaps. This observation indicates that the presence of gold nanoparticles at doping concentrations up to 2.5 % (w/w) does not significantly contribute to the permittivity of the composite. A strong impact of nanoparticle doping is found for the bulk resistance R_{LC}, as it drops from 306.2 MΩ for the pristine host 5CB to 8.5 MΩ for 0.5% (w/w) **NP1** or 73.9 kΩ for 2.5 % (w/w) **NP2**.

As the decrease of R_{LC} is proportional to the increase of doping concentration, we conclude that nanoparticle doping contaminates the host material with mobile charge carriers, leading to a rise of conductivity. This increase is rather surprising, since the nanoparticles are non-conductive themselves and do not represent an obvious source for mobile charge carriers. The double layer capacitance in the EEC is determined to be about $C_{DL} = 9.5 \pm 1.0 nF$, with no clear correlation to the nanoparticle concentration. As C_{DL} is three orders of magnitude larger than the bulk capacitance, it dominates the impedance spectra at sufficiently low frequencies. Such behavior is well reported as electrode polarization for confined liquid crystals[26–29] and can play an important role for the electro-optical performance.

4 Electrode Polarization

Electrode polarization in liquid crystal test cells is the formation of space charge regions in the vicinity of the electrodes by drifting charge carriers under the influence of an external low-frequent electric field. A visualization of this process can be found in the video in the ESI†. When the polarity of the external field changes slowly enough for the mobile charged species to be dragged towards the oppositely charged interfaces, a space charge in the vicinity of the electrodes is formed due to the confinement, significantly increasing the permittivity of the sample. At sufficiently high driving frequencies, however, the polarity changes too fast for mobile charge carriers to respond, their position essentially stationary. Thus a space charge is not formed. The transition from high to low frequency behavior is visible in the impedance response by a soft step function in ε', the real part of the permittivity ε, and a maximum in the imaginary part ε''. This Debye-type relaxation behavior is exemplified in Fig. 3, which shows the complex permittivity $\varepsilon = \varepsilon' + i\varepsilon''$ and the dielectric loss tangent $\tan\delta = \frac{\varepsilon''}{\varepsilon'}$ of a dispersion containing 0.025 % (w/w) **NP1** in 5CB. It is important to notice that the strong increase of ε' is not related to the dipolar relaxation of molecules or the impact of nanoparticles on the nematic order parameter, but rather caused by an increased number of mobile charge carriers responding to the external field. The observed increase of permittivity therefore resembles the effective permittivity of the test cell, explicitly considering charge accumulation at the interfaces. It is not connected to molecular relaxation processes in the dielectric medium.

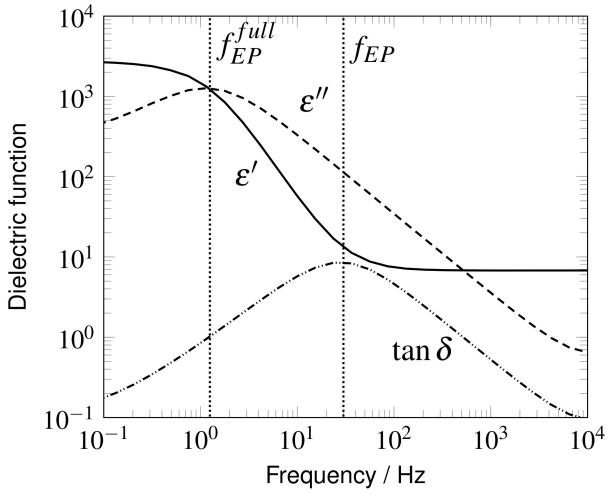

Fig. 3 Permittivity spectrum for a dispersions of 0.025 % NP1 in 5CB, exemplifying the behavior of ε', ε'' and $\tan\delta$ in the presence of electrode polarization: The onset frequency for electrode polarization f_{EP} is given by a maximum in $\tan\delta$, while the frequency of its full development f_{EP}^{full} shows a maximum in ε''. In between, a significant gain of ε' over two orders of magnitude is observed.

A detailed theoretical description for this polarization process in insulating confined media was initially derived by Macdonald[30,31]. As this general description is rather complicated and therefore inconvenient for practical use, we utilize a simplified model introduced by Coelho[32,33], which is sufficient in our case to reproduce the impedance characteristics. According to this model, the onset frequency of electrode polarization is given by

$$f_{EP} = \frac{\sigma_0}{2\pi \cdot \varepsilon_r \varepsilon_0} \sqrt{\frac{2\lambda_D}{d}} \qquad (1)$$

and depends on the conductivity σ_0 and permittivity ε of the dielectric material, its Debye screening length λ_D and the thickness d of the test cell[34]. At the onset frequency f_{EP} the electric loss tangent shows a maximum and the real part of the cell permittivity ε' becomes higher than the low frequency dielectric constant

Table 1 Nominal parameters for the elements of the EEC model (cf. Fig. 2) as obtained by fitting the EEC response to the experimental data

	R_{CR} [kΩ]	C_{LC} [pF]	R_{LC} [MΩ]	C_{DL} [nF]	W_{sr} [$\Omega s^{-0.5}$]	W_{sc} [$\Omega s^{-0.5}$]
pristine 5CB	3.40	22.8	306.2	7.51	$1.20 \cdot 10^9$	327.4
0.01 % NP1	3.47	23.0	42.9	9.13	$1.34 \cdot 10^9$	7.0
0.025 % NP1	4.28	22.4	26.2	10.23	$1.05 \cdot 10^9$	3.2
0.05 % NP1	3.82	22.9	14.4	9.54	$6.37 \cdot 10^8$	8.8
0.5 % NP1	3.51	23.2	8.5	8.65	$5.52 \cdot 10^8$	43.6
0.5 % NP2	4.62	21.8	0.28	10.33	$2.99 \cdot 10^8$	7.8
1.0 % NP2	4.77	21.6	0.17	9.99	$2.16 \cdot 10^8$	126.5
2.5 % NP2	4.43	22.8	0.07	10.71	$7.65 \cdot 10^7$	349.9

of the nematic host material ε_r. A full development of electrode polarization is characterized by a peak maximum in the imaginary part of the cell permittivity ε'', below which ε' reaches a plateau.

As doping with **NP1** and **NP2** significantly increases the conductivity, the onset frequency of electrode polarization f_{EP} shifts to higher frequencies. The impact of NPs on the electro-optical performance of the dispersion then differs, depending on whether the driving frequency is higher or lower than f_{EP}.

5 Impact on electro-optic performance

Liquid crystal test cells and LC displays are typically electrically addressed at mid-range frequencies between 100 Hz to 10 kHz. At lower frequencies flickering of light intensity occurs due to the dielectric reorientation of LC molecules following the electric field, while at higher frequencies the resistivity of connectors and ITO-electrodes as well as the onset of molecular dipole relaxations reduce the performance of the LC device. A test frequency of 1 kHz is very common for probing the electro-optic performance of nematic liquid crystals.[9,19,35,36].

In this section we discuss the impact of nanoparticle doping on the electro-optical performance and differentiate between driving frequencies above f_{EP} and lower frequencies with electrode polarization present.

5.1 Permittivity and dielectric anisotropy

For frequencies above f_{EP}, our experimental results reveal that the presence of metallic nanoparticles **NP1** or **NP2** does not noticeably affect the permittivity, as shown by the coinciding data points for $\varepsilon_\perp$ and $\varepsilon_\parallel$ at high frequencies in Figure 4. This is an expected outcome, because the volume filling factor of nanoparticles in the dispersions is well below 10^{-3} even for the highest doping concentration of 2.5 % (w/w) used in this study. According to an effective medium approach[37], the influence of the dopant permittivity should be negligible. A detailed discussion can be found in the ESI†.

At frequencies below f_{EP} the formation of space charges in the vicinity of the electrodes leads to a strong increase of permittivity, spanning several orders of magnitude. For the host 5CB the onset frequency for electrode polarization is found to be higher for homeotropic than for planar alignment, thus the rise in $\varepsilon_\parallel$ takes place at higher frequencies than for $\varepsilon_\perp$. Consequently two possible effects can be observed: (i) When the test frequency lies between the onset frequencies f_{EP} for planar and homeotropic alignment, respectively, an apparent increase of dielectric anisotropy $\Delta\varepsilon = \varepsilon_\parallel - \varepsilon_\perp$ can be observed, since only $\varepsilon_\parallel$ is affected by electrode polarization. Also for the case that the test frequency lies below f_{EP} for both principal alignments $\Delta\varepsilon$ appears enlarged, since the gain in $\varepsilon_\parallel$ is more pronounced than for $\varepsilon_\perp$. (ii) When several samples with identical alignment but different doping concentration (thus different conductivity) are compared and the test frequency lies below f_{EP} for at least one sample, a seemingly strong impact of nanoparticles on the permittivity can be observed. For both scenarios, however, the observations are not related to the dipolar relaxation of LC molecules or a variation of nematic order parameter, but rather to the formation of space charges.

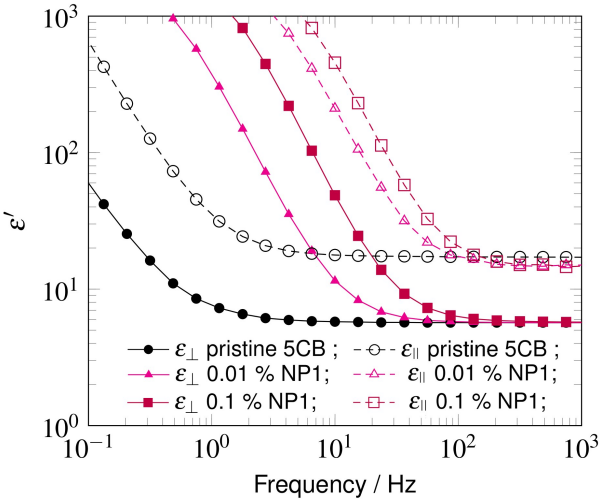

Fig. 4 Permittivity spectra showing the frequency evolution of $\varepsilon_\perp$ and f $\varepsilon_\parallel$ for prisitne 5CB and NP-LC dispersions containing 0.01 % (w/w) and 0.1 % (w/w) NP1, respectively. The significant increase of permittivity caused by electrode polarization shifts to higher frequencies with increasing doping concentration, this shift is more pronounced for $\varepsilon_\parallel$ than for $\varepsilon_\perp$.

Especially for thin test samples ($< 4\ \mu$m) and high doping concentrations f_{EP} may be close to the standard test frequency of 1 kHz. We believe a variation of test frequency to higher values can be very valuable for the interpretation of permittivity data of NP-LC nanocomposites.

5.2 Threshold Voltage

The threshold voltage V_{Th} is typically used as a measure of the ratio between the electric torque, that couples to the dielectric anisotropy and tends to reorient the director field, and the restoring elastic torque connected to the bulk elasticity. Any doping induced change of V_{Th} can then be interpreted either as a change

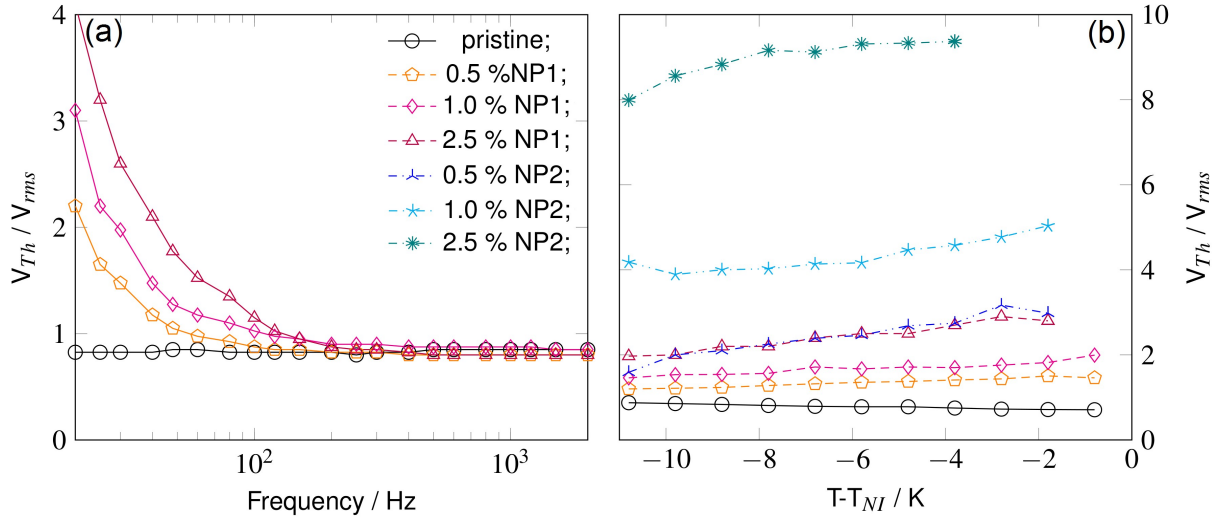

Fig. 5 Impact of electrode polarization on the threshold voltage: (a) Frequency dependence of V_{Th} for NP1-dispersions with high doping concentrations (0.5 % - 2.5 % (w/w)) in test cells with 50 μm cell gap. (b) Temperature evolution of V_{Th} in 4 μm test cells at a fixed test frequency of 1 kHz.

of bulk elasticity, of dielectric anisotropy, or both. However, such an argument only holds for driving frequencies higher than f_{EP}, as it presumes a linear relationship between applied voltage and electric field strength $E = \frac{V}{d}$. In the presence of electrode polarization, the accumulation of mobile charge carriers in the vicinity of the electrodes leads to a strongly nonlinear relation between applied voltage and electric field distribution through the cell gap and causes an effective reduction of electric field in the center of the liquid crystal[32,34] (See ESI† for further discussion). Consequently, the external voltage necessary to induce a director reorientation strongly increases for frequencies below f_{EP}, as shown for **NP1** doped 5CB filled in 50 μm test cells (see Figure 5 (a)).

The threshold V_{Th} of the pristine host 5CB is 850 $\pm$ 25 mV at 298 K and invariant over frequency. Dispersions doped with **NP1** nanoparticles show a strong increase of V_{Th} at low frequencies, while at frequencies above 300 Hz the value coincides with that of the pristine host. As LC test cells and LCD applications typically feature cell gaps thinner than 50 μm, the onset frequency of this strong increase in threshold is expected to shift to higher frequencies (see eq. 1). For illustration, V_{Th} at 1 kHz for dispersions of **NP1** and **NP2** in 4 μm test cells as a function of temperature is shown in Figure 5 (b). The threshold voltage is significantly increased for doped samples compared to the pristine host since $f_{EP} > 1$ kHz for all dispersions. This gain is however not related to the elasticity or dielectric anisotropy of the LC material, but results from space charges and electrode polarization. The ascent of V_{Th} with increasing temperatures indicates a slight shift of f_{EP} to higher frequencies, presumably caused by non-identical temperature dependencies of permittivity ε and conductivity σ_0.

6 Conclusions

We have shown by the analysis of impedance spectra that doping a nematic host with organically functionalized gold nanoparticles significantly decreases the bulk resistivity by several orders of magnitude. This doping effect correlates to an increased number of mobile charge carriers and is found to be more pronounced for mesogenic functionalized NPs than for alkylthiol functionalized particles. The NP-induced increase of conductivity leads to the formation of electrode polarization at low driving frequencies, which deteriorates the electro-optical performance. As an example we demonstrated the different impact of nanoparticle doping on the threshold voltage V_{Th} and permittivity ε for driving frequencies above and below the onset frequency for the formation of electrode polarization, respectively. While the electro-optical parameters remain unaffected at higher driving frequencies, significantly higher threshold voltages and permittivities for doped samples are observed in the low frequency regime. We demonstrated that the onset of electrode polarization shifts to higher frequencies for increased conductivity and thinner sample thickness and thus may even affect the electro-optical performance of applications at a standard driving frequency of 1 kHz. Beyond our study for the nematic phase of 5CB, we expect that also in higher ordered mesophases a NP-doping related contamination with mobile charge carriers leads to the formation of electrode polarization and consequently deterioates the electro-optic performance. Hence, our results are also of importance for electro-optical switching in smectic or blue phase applications. Future work will have to address the origin of mobile charge carriers, as this will help to adjust NP synthesis and composite mixing strategies to match low conductivtiy requirements for NP-LC composites with high electro-optical performance.

Financial support by the Fonds National de la Recherche Luxembourg (FNR-AFR project "Disgona" No 9170337) is gratefully acknowledged.

References

1 E. Ouskova, O. Buchnev, V. Reshetnyak, Y. Reznikov and H. Kresse, *Liquid Crystals*, 2003, **30**, 1235–1239.

2 F. Li, O. Buchnev, C. I. Cheon, A. Glushchenko, V. Reshetnyak, Y. Reznikov, T. J. Sluckin and J. L. West, *Physical Review Letters*, 2006, **97**, 5–8.

3 S. Sridevi, S. K. Prasad, G. G. Nair, V. D'Britto and B. L. V. Prasad, *Applied Physics Letters*, 2010, **97**, 1346–56.

4 G. Scalia, J. P. F. Lagerwall, S. Schymura, M. Haluska, F. Giesselmann and S. Roth, *Physica Status Solidi (B) Basic Research*, 2007, **244**, 4212–4217.

5 I. Dierking, G. Scalia and P. Morales, *Journal of Applied Physics*, 2005, **97**, 1–5.

6 A. García-García, R. Vergaz, J. F. Algorri, X. Quintana and J. M. Otón, *Beilstein Journal of Nanotechnology*, 2015, **6**, 396–403.

7 J. Mirzaei, M. Urbanski, H.-S. Kitzerow and T. Hegmann, *ChemPhysChem*, 2014, **15**, 1381–1394.

8 M. Urbanski, *Liquid Crystals Today*, 2015, **24**, 102–115.

9 M. Urbanski, J. Mirzaei, T. Hegmann and H.-S. Kitzerow, *ChemPhysChem*, 2014, **15**, 1395–1404.

10 J. Mirzaei, M. Urbanski, H.-S. Kitzerow and T. Hegmann, *Phil. Trans. R. Soc. A*, 2013, **371**, 20120256.

11 S. Kobayashi, T. Miyama, N. Nishida, Y. Sakai, H. Shiraki, Y. Shiraishi and N. Toshima, *J. Display. Tech.*, 2006, **2**, 121–129.

12 H. Yoshida, K. Kawamoto, H. Kubo, T. Tsuda, A. Fujii, S. Kuwabata and M. Ozaki, *Advanced Materials*, 2010, **22**, 622–626.

13 T. Zhang, C. Zhong and J. Xu, *Japanese Journal of Applied Physics*, 2009, **48**, 055002.

14 S. Tomylko, O. Yaroshchuk, O. Kovalchuk, U. Maschke and R. Yamaguchi, *Ukr. J. Phys.*, 2012, **57**, 239–243.

15 Y.-S. Ha, H.-J. Kim, H.-G. Park and D.-S. Seo, *Optics express*, 2012, **20**, 6448–55.

16 A. García-García, R. Vergaz, J. F. Algorri, M. A. Geday and J. M. Otón, *Journal of Physics D: Applied Physics*, 2015, **48**, 375302.

17 H. Qi and T. Hegmann, *Journal of Materials Chemistry*, 2006, **16**, 4197.

18 H. Qi and T. Hegmann, *Liquid Crystals Today*, 2011, **20**, 102–114.

19 M. Draper, I. M. Saez, S. J. Cowling, P. Gai, B. Heinrich, B. Donnio, D. Guillon and J. W. Goodby, *Advanced Functional Materials*, 2011, **21**, 1260–1278.

20 M. Wojcik, M. Kolpaczynska, D. Pociecha, J. Mieczkowski and E. Gorecka, *Soft Matter*, 2010, **6**, 5397.

21 W. W. Weare, S. M. Reed, M. G. Warner and J. E. Hutchison, *J. Am. Chem. Soc.*, 2000, **122**, 12890–12891.

22 *Electroopic effect in liquid crystal materials Metamaterials*, ed. B. A. Blinov and V. G. Chigrinov, Springer, New York, 1996.

23 G. J. Sprokel, *Molecular Crystals and Liquid Crystals*, 1974, **26**, 45–57.

24 B. A. Belyaev and N. A. Drokin, *Physics of the Solid State*, 2015, **57**, 181–187.

25 J. Illig, *PhD thesis*, Karlsruher Institut für Technologie, 2014.

26 H. Mada and M. Ryuzaki, *Japanese Journal of Applied Physics, Part 2: Letters*, 1995, **34**, year.

27 S. Murakami, H. Iga and H. Naito, *Journal of Applied Physics*, 1996, **80**, 6396.

28 A. L. Alexe-Ionescu, G. Barbero and I. Lelidis, *Physical Review E - Statistical, Nonlinear, and Soft Matter Physics*, 2009, **80**, 1–6.

29 G. Barbero and A. L. Alexe-Ionescu, *Liquid Crystals*, 2005, **32**, 943–949.

30 J. R. Macdonald, *Physical Review*, 1953, **92**, 4–17.

31 J. R. Macdonald, *The Journal of Chemical Physics*, 1954, **22**, 1857.

32 R. Coelho, *Revue Phys. Appl.*, 1983, **18**, 137–146.

33 R. Coelho, *Journal of Non-Crystalline Solids*, 1991, **131-133**, 1136–1139.

34 R. J. Klein, S. Zhang, S. Dou, B. H. Jones, R. H. Colby and J. Runt, *Journal of Chemical Physics*, 2006, **124**, 1–8.

35 S. Khatua, P. Manna, W. S. Chang, A. Tcherniak, E. Friedlander, E. R. Zubarev and S. Link, *Journal of Physical Chemistry C*, 2010, **114**, 7251–7257.

36 U. B. Singh, R. Dhar, R. Dabrowski, M. B. Pandey and P. Taylor, *Liquid Crystals*, 2013, **40**, 774–782.

37 *Optical Metamaterials*, ed. W. Cai and V. Shalaev, Springer, New York, 2010.

We show how the contamination with mobile charge carriers caused by nanoparticle doping affects the dielectric response of a nematic host material and deteriorates its electro-optic performance.